Does Translational Symmetry Matter on the Micro Scale? Fibroblastic and Osteoblastic Interactions with the Topographically Distinct Poly(ε-caprolactone)/Hydroxyapatite Thin Films

Vuk Uskoković*,†,‡ and Tejal A. Desai*,†

†Therapeutic Micro and Nanotechnology Laboratory, Department of Bioengineering and Therapeutic Sciences, University of California, San Francisco, San Francisco, California 94158-2330, United States

‡Advanced Materials and Nanobiotechnology Laboratory, Department of Bioengineering, University of Illinois, Chicago, Illinois 60607-7052, United States

ABSTRACT: Material composition and topography of the cell-contacting material interface are important considerations in the design of biomaterials at the nano and micro scales. This study is one of the first to have assessed the osteoblastic response to micropatterned polymer–ceramic composite surfaces. In particular, the effect of topographic variations of composite poly(ε-caprolactone)/hydroxyapatite (PCL/HAp) films on viability, proliferation, migration and osteogenesis of fibroblastic and osteoblastic MC3T3-E1 cells was evaluated. To that end, three different micropatterned PCL/HAp films were compared: flat and textured, the latter of which included films comprising periodically arranged and randomly distributed oval topographic features 10 μm in diameter, 20 μm in separation and 10 μm in height, comparable to the dimensions of MC3T3-E1 cells. PCL/HAp films were fabricated by the combination of a bottom-up, soft chemical synthesis of the ceramic, nanoparticulate phase and a top-down, photolithographic technique for imprinting fine, microscale features on them. X-ray diffraction analysis indicated an isotropic orientation of both the polymeric chains and HAp crystallites in the composite samples. Biocompatibility tests indicated no significant decrease in their viability when grown on PCL/HAp films. Fibroblast proliferation and migration onto PCL/HAp films proceeded slower than on the control borosilicate glass, with the flat composite film fostering more cell migration activity than the films containing topographic features. The gene expression of seven analyzed osteogenic markers, including procollagen type I, osteocalcin, osteopontin, alkaline phosphatase, and the transcription factors *Runx2* and *TGFβ-1*, was, however, consistently upregulated in cells grown on PCL/HAp films comprising periodically ordered topographic features, suggesting that the higher levels of symmetry of the topographic ordering impose a moderate mechanochemical stress on the adherent cells and thus promote a more favorable osteogenic response. The obtained results suggest that topography can be a more important determinant of the cell/surface interaction than the surface chemistry and/or stiffness as well as that the regularity of the distribution of topographic features can be a more important variable than the topographic features per se.

KEYWORDS: *calcium phosphate, controlled drug delivery, hydroxyapatite, nanoparticles, photolithography, poly(ε-caprolactone), topography, X-ray diffraction*
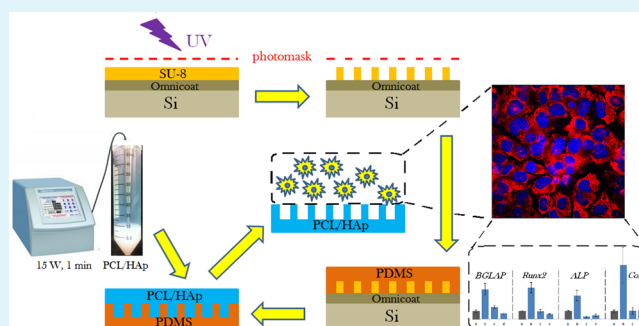
1. INTRODUCTION

Optimization of the cell/material interface presents a major aspect of the design of biomaterials for specific therapeutic and/or diagnostic applications. The biomaterial surface is a key determinant of the attachment of cells and the physisorption of macromolecular species, the effects on which the biological fate of the material greatly depends. For example, implantation of a bone substitute that sustainably supplements an infected bone with an antibiotic presents an onset of the so-called "race for the surface" that involves bone cells and bacteria.[1] Both the winner of this race and the outcome of the therapy are often decided by the surface properties of the material. Delineating the surface properties that boost the affinity and proliferation of

bone cells is thus of great interest for advanced bone engineering applications.

In addition to chemical, crystallographic and mechanical surface properties, its topography is another important consideration in the design of biomaterials at the molecular scale. Previously, it has been demonstrated that moderately rough surfaces frequently favor the attachment and proliferation of several different cell types compared to flat surfaces.[2−4] Titanium implants with naturally smooth surfaces have thus
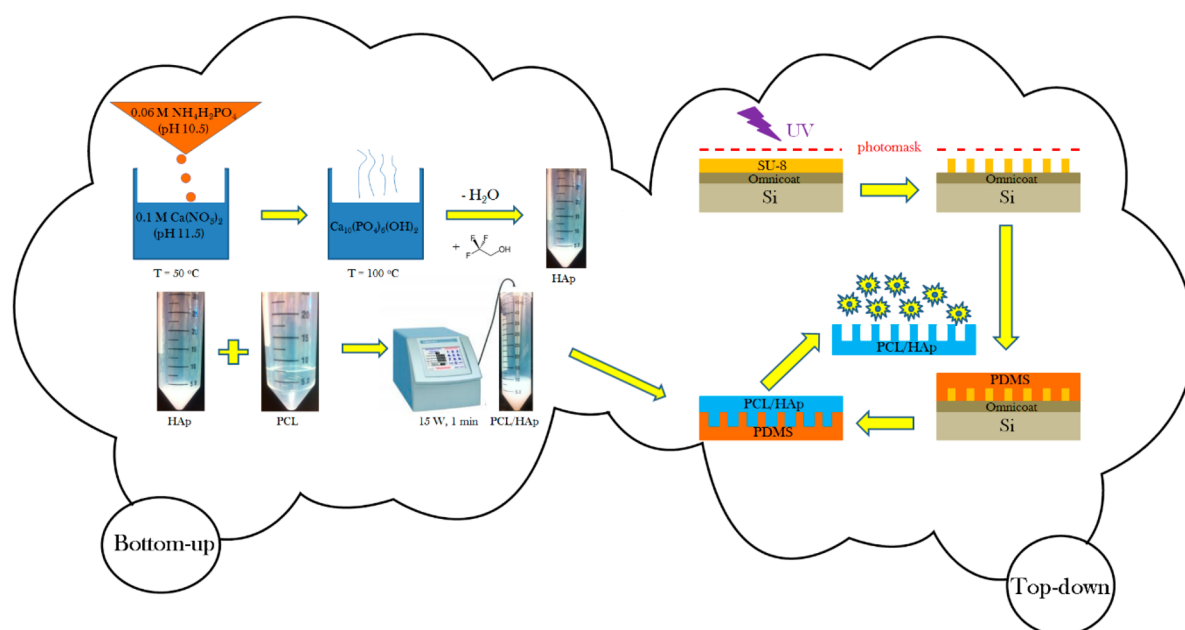
Figure 1. Schematic description of the fabrication of PCL/HAp films using a combination of bottom-up and top-down synthetic techniques.

been comparatively ineffective in tissue adhesion; to enhance their integration with the body, they are often subjected to sandblasting and/or acid etching prior to implantation.[5,6] In fact, the proliferation rate of human bone marrow-derived mesenchymal cells on abraded titanium surfaces was even higher than on smooth titanium coated with bioactive layers of hydroxyapatite (HAp), suggesting that topography can out-weigh chemistry when it comes to a search for biomaterial properties for an ideal osseointegration.[7] A systematic review of works published on the effect of titanium surface topography on bone integration concluded that smooth and minimally rough surfaces had demonstrated consistently weaker bone-to-implant contacts than rougher surfaces.[8] Gas plasma treatment of borosilicate glass coverslips can remove the surface islands with ca. 1–3 μm in diameter and 1–3 nm in height and thus render them incapable of providing a surface for the attachment and proliferation of fibroblasts.[9] Molecular adsorption mecha-nisms are, in fact, driven by the Gibbs isotherm, which dictates that the greater the surface energy, the greater the adsorption. Hydrogen adsorption capacity, for example, becomes markedly enhanced as one shifts from using perfectly ordered carbon crystals on the atomic scale to those containing topological defects,[10] whereas no adsorption of carbon monoxide was detected on atomically smooth gold.[11] Owing to the quantum confinement effect and anisotropic surface energy, atomic smoothness in thin films and nanostructures in general is, in fact, a metastable state, which, upon annealing, transforms to a thermodynamically stable, but roughened state comprising surface clusters whose size and shape are defined through the structural magic numbers.[12]

Because cell attachment is preceded by the adsorption of cell adhesion proteins, it also tends to proceed more facilely on topographically uneven surfaces. For example, the proliferation rate and the expression of alkaline phosphatase were higher for osteoblastic MC3T3-E1 cells on etched alumina than on a polished one.[13] Other studies have shown that rough surfaces favor the adhesion of osteoblasts,[14] osteogenesis[15] and osseointegration of the implant.[16] One such irregular top-ography typifies biological apatite due to its intrinsic nano-

particulate nature.[17] Bone remodeling involves coordinated action of different cell types and resorption pits created by osteoclasts are thought to present an important factor that facilitates the adhesion of osteoblasts to the bone.[18] Consequently, introduction of nanosized grooves onto polystyrene substrates boosted the gene expression of osteocalcin, collagen type I and β1-integrin, leading to higher levels of bone mineral formation.[19] Topographically irregular, unsmooth surfaces were also able to enhance the differentiation of mesenchymal stem cells (MSCs) into osteoblasts.[20,21] An increase in the distance between periodically arranged 700 nm wide polyurethane posts from 1.7 to 4.9 μm was also able to change the fate of MSCs from adipogenic to osteogenic.[22] Moreover, a combination of (a) microroughness with (b) nanoscopic topographic elements induced a higher production of osteopontin in MC3T3-E1 cells than accomplished by a or b alone.[23] All these studies combined confirm that topography at both micro and nano scales is as important in the biomaterials design as chemistry and mechanical properties.

The design of multifunctional composite materials is important for the next generation of biomedical implants or tissue scaffolds. Bone is an example of one such material, as the strengths of both of its components compensate for the weaknesses of each, i.e., HAp imparts high elastic modulus and compressive strength to the bone, whereas collagen yields toughness, elasticity and moderate tensile strength to it. Polymer/HAp composites present one class of artificial composite materials that has attracted the particular attention of bone engineers owing to their wide range of unique properties, particularly in terms of their ability to emulate the soft/hard composite structure of bone. HAp, on one hand, presents an ideal hard component of bone tissue substitutes, given the fact that it already comprises the great majority of bone (70 wt %) as well as that it is (i) biocompatible, (ii) bioactive, (iii) tunable to a wide window of biodegradation rates,[24] (iv) capable of binding comparatively large amounts of organic molecules via adsorption,[25] (v) able to facilitate endosomal escape,[26] (vi) osteoconductive, but also (vii) osteoinductive for specific particle structures and dosages.[27,28]

Combinations of HAp with poly(ε-caprolactone) (PCL), the polyester used in this study, have, for example, resulted in the improved tensile strength of the ceramic phase and the improved elastic modulus of the polymeric phase by several orders of magnitude.[29−31] Additionally, complementing a ceramic powder with a viscous polymeric phase allows for the direct injection of the former to the bony defect, bypassing the need for surgical implantation. Then, polymeric layers are potentially able to stabilize the drug physisorbed on the HAp surface and prevent its burst release.[32] More sustained and multiple stage release profiles could thus be also obtained.[33] The hydrolysis of polyesters also exposes carboxylic acid moieties to the local biological environment,[34] but this acidification effect, known to have caused bone resorption in the past,[35] could be compensated for by synchronizing their degradation with that of alkaline HAp.[36]

In this study, we have looked at how topographical variations of PCL/HAp films affect the behavior of fibroblastic and osteoblastic cells cultured on them. To that end, we compared three different PCL/HAp surfaces: flat and textured, the latter of which included films comprising periodically arranged and randomly distributed topographic features. Only a few studies so far have dealt with the osteoblastic response to micro-patterned polymeric surfaces[37−39] and this is one of the first studies of this type involving a polymer−ceramic composite.[40] The method used to fabricate these composite films was a combination of a bottom-up, soft chemical synthesis of their ceramic, nanoparticulate phase and a top-down, photolithographic technique for imprinting fine, microscale features on them. Both of these approaches to synthesis of fine structures suffer from inherent weaknesses, such as difficult integration of products into device components in the case of the former and relative robustness, expensiveness and massive equipment in the case of the latter.[41] Probing of the middle-ground synergies between the two, which may help to overcome each other's downsides, is thus of vital importance for the field of materials science and engineering and presents another unique aspect of this study.

2. MATERIALS AND METHODS

2.1. Synthesis of PCL/HAp Films. A schematic description of the fabrication of PCL/HAp composite films based on a combination of bottom-up and top-down processing is presented in Figure 1. The composite films with specifically designed surface features were prepared by a photolithographic method. Two blueprints for the photomasks were created in AutoCAD (Autodesk, Inc., 2013), one of which was composed of translationally symmetrical circles with 10 μm in diameter and 20 μm in separation, and the other one of which comprised identical circles, but randomly arranged in 2D. The surface density of topographic features was the same on both the ordered and randomized substrates: 1200 circles per mm². Custom photomasks were made from Teflon based on the given blueprints (CAD/Art Services, Inc.). A layer of Omnicoat (MicroChem) was spin-cast at 500 rpm and the ramp speed of 100 rpm/sec for 5 s and at 3000 rpm and the ramp speed of 300 rpm/sec for 30 s onto a round silicon wafer (Addison Engineering, Inc.) with 380 μm in thickness, 3″ in diameter and ⟨111⟩ crystal planes exposed on the surface using a PMW32 spin coater (Headway Research) and baked for 1 min at 200 °C. After the silicon wafer cooled, a layer of SU-8 2005 negative photoresist (Microchem) was spin-cast onto the Omnicoat-covered silicon wafer first at 500 rpm and the ramp speed of 100 rpm/sec for 10 s and then at 1000 rpm and the ramp speed of 300 rpm/sec for 30 s, and then prebaked at 95 °C for 3 min. An array of micropillars was then patterned into the photoresist using the Teflon photomask and exposing the photoresist to UV light for 30 s at the intensity of 11

mW/cm² using a Karl Suss MJB 3 mask aligner (SUSS MicroTec). The SU-8 molds were then postbaked at 95 °C for 4 min and the photoresist unexposed to UV irradiation was dissolved in gently agitated SU-8 Developer (Microchem) in a Petri dish for 3 min. The wafers were then rinsed with isopropyl alcohol and dried at 95 °C for 30 s. Such prepared master stamps were used as inverse templates for the fabrication of poly(dimethylsiloxane) (PDMS) films. The PDMS base (Sylgard 184 Silicone, dimethylvinyl-terminated) and the curing agent were mixed in a 10:1 weight ratio and degassed under vacuum for 30 min. Ten grams of such mixture were poured onto a single SU-8 micropatterned wafer, degassed for additional 30 min and then baked at 65 °C for 1 h. Once cured, the PDMS was peeled from the silicon master. The obtained PDMS layer was then used as an inverse template for the fabrication of PCL/HAp composite films.

Narrowly dispersed spherical HAp nanoparticles were first prepared by adding 150 mL of 0.06 M aqueous solution of $NH_4H_2PO_4$ containing 7 mL of 28% NH_4OH dropwise to the same volume of 0.1 M aqueous solution of $Ca(NO_3)_2$ containing 15 mL of 28% NH_4OH, while vigorously stirring with a magnetic bar (400 rpm) and keeping the suspension on a plate heated to 50 °C. After the addition of $NH_4H_2PO_4$ was complete, the suspension was brought to boiling, then immediately removed from the heater and let cool in air. Stirring was suspended and the precipitate alongside its parent solution was left to age in atmospheric conditions for 24 h. After the given time, the precipitate was centrifuged (3 min at 3500 rpm) and the supernatant was decanted. The precipitate was then washed with distilled water to eliminate the excess alkali and the centrifugation and decantation procedure was repeated. Three milliliters of the resulting gelatinous HAp precipitate were then mixed with 3 mL of 2,2,2-trifluoroethanol and vortexed (Thermolyne Maxi Mix II) for 10 s. Three milliliters of the resulting colloidal suspension of HAp (3 mL) were then added to 7 mL of the previously prepared, 100 mg/mL solution of 80 kDa PCL in 2,2,2-trifluoroethanol, and the solution was agitated for 1 min in an ultrasound field using a Q700 QSonica ultrasonicator with a 1/8″ tip, the power of 15 W and the overall delivered energy of 1 kJ. The given PCL solution was made by dissolving the polymer (M_w = 80−100 kDa) in 2,2,2-trifluoroethanol under mild agitation for 3 h at 65 °C. The resulting colloidal suspension of HAp and PCL in a 1:5 weight ratio was poured over the PDMS films and let dry in the atmospheric conditions for 2 h, after which the PCL/HAp films were peeled off the PDMS surface with forceps and used for in vitro cell experimentation.

2.2. Characterization of PCL/HAp Films. The morphology of PCL/HAp films was characterized on an Olympus BX60 optical microscope equipped with a Zeiss AcioCam MRm camera and on a Carl Zeiss Ultra 55 field-emission scanning electron microscope at the voltage of 2 kV. The samples were sputtered with iridium (∼3 nm) prior to observation. PCL/HAp films were also characterized on an Ambios Technology XP-2 Stylus Profiler (Santa Cruz, CA). The profilometry analysis was performed using the scan speed of 50 μm/sec, the scan length of 0.5 mm, and the stylus force of 0.5 mg. X-ray diffraction analysis in the transmission mode was performed on a Bruker Advanced D-8 diffractometer equipped with a Johansson monochromator in the 2θ range of 8−70° and the scan step of 0.05°. X-ray diffraction analysis in the reflection mode was performed on a Philips 1050 diffractometer using the Bragg−Brentano parafocusing method and the same 2θ range and scanning resolution. The most intensive reflections, (110) for PCL and (211) for HAp, were used to estimate the average crystallite size (d) for the two components using the Debye−Scherrer equation in the following form, with $\beta_{1/2}$ being the half-width of the given diffraction peak (in radians), θ being the diffraction angle and λ being the wavelength of Cu Kα as the radiation source (1.5418 Å):

$$d = 0.94\lambda/\beta_{1/2}\cos\theta$$

2.3. Model Drug Loading and Release. Fluorescein sodium ($C_{20}H_{10}Na_2O_5$; log P = 3.4; M_w = 376.28 g/mol, d ∼ 0.7 nm, Fluka) was used as a small molecule model drug in this study. One milliliter of 20 mg/mL fluorescein−Na dissolved in 2,2,2-trifluoroethanol was added to 4 mL of the aforementioned PCL/HAp mixture, vortexed and poured over the PDMS substrates. After the films dried, they were

Table 1. Primer pair sequences used for the qPCR analysis

gene	forward 5′-3′ primer	reverse 5′-3′ primer
ACTB	GGCCCAGAGCAAGAGAGGTATCC	ACGCACGATTTCCCTCTCAGC
BGLAP	CTCACAGATGCCAAGCCCA	CCAAGGTAGCGCCGGAGTCT
Runx2	AAATGCCTCCGCTGTTATGAA	GCTCCGGCCCACAAATCT
ALP	TCCTGACCAAAAACCTCAAAGG	TGCTTCATGCAGAGCCTGC
Col I	GCGAAGGCAACAGTCGCT	CTTGGTGGTTTTGTATTCGATGAC
BSP-1	AGGAGGAGGCAGAGCACA	CTGGTATGGCACAGGTGATG
TGFβ-1	AGCCCGAAGCGGACTACTAT	TCCCGAATGTCTGACGTATTG

removed with the forceps. Model drug release experiments were conducted by immersing 5 mg of such prepared fluorescein-loaded PCL/HAp films in 5 mL of phosphate buffered saline (PBS, pH 7.4) and incubating them in the dark at 37 °C with no agitation for up to 1 month. Every 24–48 h, 10 μL aliquots were sampled, mixed with 90 μL of PBS and analyzed for fluorescence (Packard Fluorocount, $\lambda_{excitation}$ = 495 nm, $\lambda_{emission}$ = 525 nm) convertible to the concentration of the released fluorophore. After 2 months, fluorescein-loaded PCL/HAp films were dissolved by adding 2 mL of 2,2,2-trifluoroethanol to the solutions containing them and incubating overnight at 37 °C. The resulting fluorescence was measured and used to calculate the overall amount of the model drug initially contained by the films. Each sample was analyzed in triplicates and the fluorescence of each experimental replica was determined as the average of three independent measurements.

2.4. Cell Culture. Mouse calvarial preosteoblastic cell line, MC3T3-E1 subclone 4, was purchased from American Tissue Culture Collection (ATCC, Rockville, MD) and cultured in Alpha Minimum Essential Medium (α-MEM; Gibco) supplemented with 10% fetal bovine serum (FBS, Invitrogen) and no ascorbic acid (AA). The medium was replaced every 48 h, and the cultures were incubated at 37 °C in a humidified atmosphere containing 5% CO_2. Every 7 days, the cells were detached from the surface of the 75 cm² cell culture flask (Greiner Bio-One) using 0.25 wt % trypsin, washed, centrifuged (1000 rpm × 3 min), resuspended in 10 mL of α-MEM and subcultured in a 1:7 volume ratio. Cell passages 21–27 were used for the experiments reported here. The cultures were regularly examined under an optical microscope to monitor growth and possible contamination.

PCL/HAp films were cut with a scalpel in the shape of 48- or 96-well plates, placed into them and sterilized via exposure to UV light for 1 h. Before positioning the film inserts into the wells, their bottoms were glazed with silicone sealant, which helped in gluing them to the bottom of the wells. MC3T3-E1 cells were then seeded on the films at the density of 3 × 10⁴ cells/cm² and in 250 μL/cm² of the above-mentioned medium. The medium was replaced every 48 h, and the cultures were incubated at 37 °C in a humidified atmosphere containing 5% CO_2.

2.5. MTT and Proliferation Assays. For the purpose of MTT (3-(4,5-dimethylthiazol-2-yl)-2,5-diphenyltetrazolium bromide) in vitro toxicological assay, MC3T3-E1 cells were seeded on PCL/HAp films in 48-well plates and cultured in 180 μL of the above-mentioned AA-free medium for different periods of time. The AA-free medium was replaced every 48 h. At the end of the incubation period, 20 μL of 5 mg/mL MTT (Sigma M-5655) in PBS were added to each well. After 4 h of incubation at 37 °C, 220 μL of MTT solubilization solution (Sigma M-5655) were added to each well. Following an additional 2 h of incubation of softly shaken wells (60 rpm) at room temperature, 100 μL aliquots from each well were analyzed for absorbance at 570 nm on a UV/vis spectrophotometric microplate reader (Molecular Devices, Spectra Max 190). All the particle types were analyzed in biological triplicates and the resulting absorbance values were normalized to the negative control. For the purpose of proliferation measurements, cells grown under the same conditions were detached after different periods of time by incubating first with 200 μL of PBS for 10 min and then with 200 μL of 0.25 wt % trypsin for an additional 10 min, after which the suspended cells were counted on a hemocytometer.

2.6. Migration Assay. The migration assay was carried out by adhering PCL/HAp films covering 50% of the bottom 12-well surface after 5 days of incubation of MC3T3-E1 cells seeded at the density of 3 × 10⁴ cells/cm². Glass slides were used as a positive control. After 3 days of additional incubation, the films were peeled off, washed with PBS and trypsinized with 0.25 wt % trypsin. The number of cells was counted on a hemocytometer and normalized to the positive control. All the PCL/HAp films were analyzed in triplicates and six independent measurements were taken of each sample.

2.7. Immunofluorescent Staining. A portion of the cells was stained after 7 days of incubation for collagen type I and nucleus. The staining procedure began with washing the cells with PBS (pH 7.4) and fixing them for 15 min in 3.7% paraformaldehyde. The cells were then washed with PBS 3 × 5 min and then with the blocking solution (PBT = 1% bovine serum albumin (BSA), 0.1% Triton X-100 in PBS) 2 × 5 min. The cells were then blocked and permeabilized in PBT for 48 h, and then incubated in 500 μL/well of the primary antibody, 10 μg/mL rabbit anticollagen-type-1 (Abcam) in PBT for 1 h. The cells were then washed with PBS 3 × 10 min and incubated with 500 μL/well of the secondary antibody, 10 μg/mL AlexaFluor 555 goat antirabbit IgG (Invitrogen) and 20 μg/mL 4′,6-diamidino-2-phenylindole dihydrochloride nuclear counterstain (DAPI, Invitrogen), all in PBT for 1 h and then washed with PBS 3 × 5 min. The coverslips containing the fixed and stained cells were mounted onto glass slides using hard set Vectashield and nail polish and were subsequently imaged on a confocal laser scanning microscope − C1si (UCSF Nikon Imaging Center) at 60× magnification in oil. The final images were obtained by z-stack volume-rendering 15−20 raw images spaced by 1 μm. All the experiments were done in triplicates.

2.8. Real-Time PCR. For the purpose of the real-time polymerase chain reaction (qPCR) analysis, MC3T3-E1 cells were first seeded on PCL/HAp films in 96-well plates at the density of 3 · 10⁴ cells per well and cultured in 100 μL of the above-mentioned AA-free medium for 48 h. The AA-free medium was then substituted with the AA-supplemented medium. After an additional 48 h incubation period, cell lysis, reverse transcription (Bio-Rad) and qPCR (Applied Biosystems, StepONEPlus) were performed using the Fast SYBR Green Cells-to-CT kit (Ambion) in accordance with the manufacturer's instructions. Each experiment was done in triplicates and each experimental replica was analyzed for mRNA expression in triplicates too ($n = 3 \times 3$). The expressions of one housekeeping gene, β-actin (ACTB), and six additional ones, including osteocalcin (BGLAP), osteopontin (BSP-1), procollagen type I (Col I), alkaline phosphatase (ALP), and the transcription factors, Runx2 and TGFβ-1 were analyzed. Table 1 shows the primer pair sequences used. The real-time PCR results were analyzed using the $\Delta\Delta C_t$ method and all the data were normalized to ACTB expression levels.

3. RESULTS AND DISCUSSION

3.1. Microstructural and Topographic Characteristics of the Composite. Blueprints of the topographic features of PCL/HAp films drawn in AutoCAD, along with the corresponding PDMS templates and SEM images of the final products, are shown in Figure 2. The PCL/HAp films were of two types: those with a high order of translational symmetry and those typified by the absence of any translational symmetry. The profilometry data presented in Figure 3a
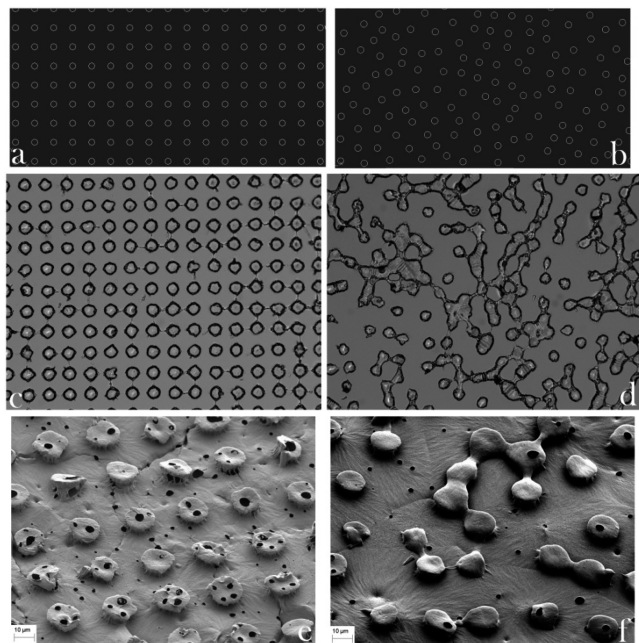
Figure 2. AutoCAD blueprints (a, b), optical images of PDMS templates with wells on their surface (c, d) and SEM images of PCL/HAp films (e, f) with ordered (a, c, e) and disordered (b, d, f) pillar-shaped topographical features. The diameter of the spherical features is 20 μm.

demonstrate the regularity and irregularity, respectively, of protuberances on the surface of the PCL/HAp films, whereas X-ray diffractograms in Figure 3b verify the presence of both HAp and PCL in the composite films. The two most intense diffraction peaks, at $2\theta = 21.5$ and $23.9°$, are derived from the (110) and (200) planes of semicrystalline orthorhombic PCL,

respectively,[42,43] whereas all other indexed peaks belong to hexagonal HAp reflections (space group $P6_3/m$). Unlike the sharp reflections of PCL, the diffraction peaks of HAp were comparatively broad and the lower limit for the crystallite size was estimated using the Debye−Scherrer equation at only 8 nm, as compared to >100 nm for PCL. Even though the addition of HAp to a PCL matrix suppressed the crystallization of the polymer,[44] crystallinity of PCL is expected to further increase with the degradation time, as the hydrolytic scission of long molecular chains leads to an increased mobility of the shorter polymeric chains and their greater tendency to adopt a more symmetric ordering in space.[45] The low crystallinity of HAp that is to be applied as a bone filler is expected to favor the resorption of the implant and its timely replacement with the newly formed bone,[46] an effect that the nanoscopic particle size additionally contributes to.[47,48] No difference was detected between diffractograms recorded in the transmission and reflection modes, suggesting that the composite films comprise an isotropic distribution of HAp crystallites (Figure 3b). Likewise, as also visible from Figure 3b, no peaks were detected during the texture analysis on the two most intense reflections for PCL and on (002) reflection of HAp ($2\theta = 25.9$), corresponding to the most probable preferential growth, along the z-axis, thus reconfirming the isotropic distribution of HAp crystallites and demonstrating that there was also no specific orientation of the polymeric chains in the sample.

Both of the textured films comprised oval surface features with the average height of 10 μm, the diameter of 10 μm and the separation length of 20 μm. These dimensions were deliberately chosen because they are comparable to the average size range of MC3T3-derived fibroblasts: 20−60 μm. Electromagnetic radiation interacts most intensely when its wavelength is comparable to the size of the physical objects that it encounters and the distance between the object's elementary constituents that it passes through (e.g., diffraction), and we
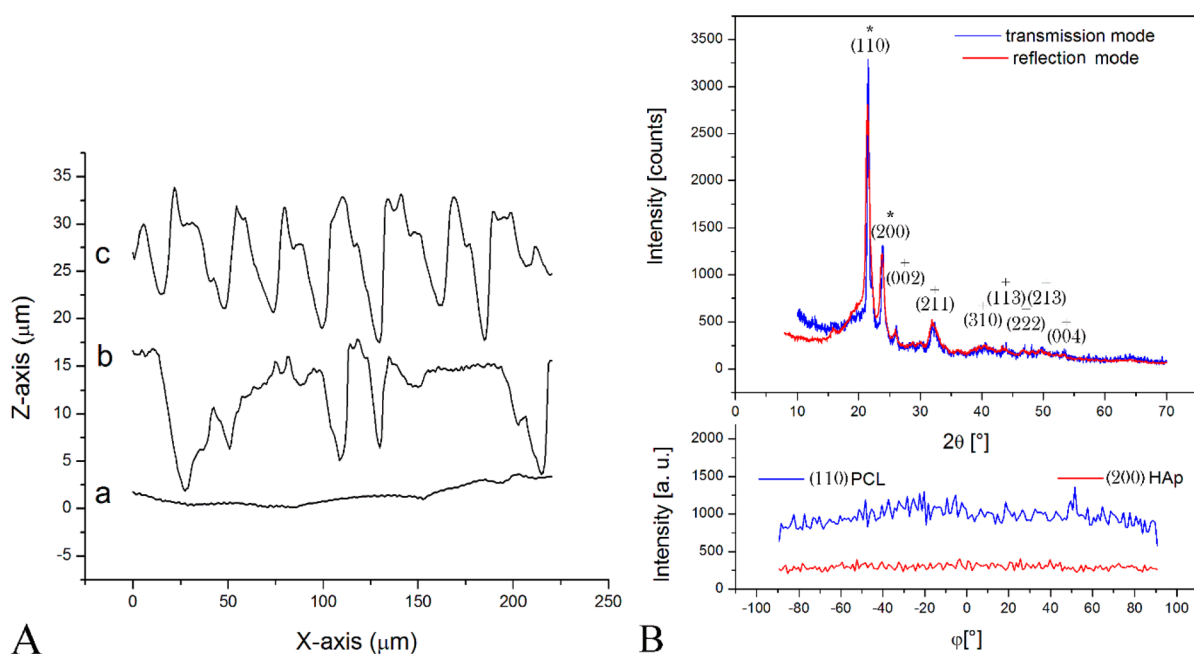

Figure 3. (A) Profilometry diagrams of three different PCL/HAp films synthesized: (a) flat; (b) topographically disordered; (c) topographically ordered. (B) X-ray diffractograms of PCL/HAp films in transmission and reflection modes and the intensity of (110) reflection of PCL and (200) reflection of HAp in PCL/HAp films as a function of the angle, φ, denoting rotation around the axis perpendicular to the sample plane in the transmission mode. Diffraction peaks indexed with * are PCL-derived, whereas those indexed with + are HAp-derived.

hypothesized that a similar principle may hold true for the interaction between cells and foreign surfaces (Figure 4). The
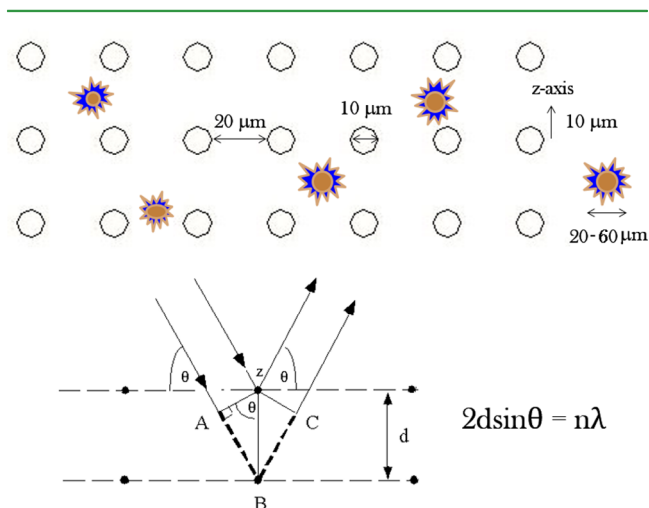

Figure 4. Size of the surface features and the distance between them were chosen to be in the same order of magnitude as that of the size of fibroblastic cells, assuming that the surface effects on the cells would be maximized thereby, in analogy with the light diffraction process, which is most intense when the spacing between the scattering entities and the wavelength of the diffracted light are in the same range, as could be seen from Bragg's equation, where λ is the wavelength of the incident X-ray photons, θ is the diffraction angle, d is the spacing between two nearest planes containing the scattering entities and n is the integer signifying the order constructive interference, with $n = 1$ being the most probable and intense one.

surface density of topographic features was chosen to be identical on both the ordered and randomized PCL/HAp substrates, equaling 1200 pillars per mm^2, so as to ensure no difference in wettability between the surfaces. Flat films, comprising no topographic features on the micrometer scale, were also produced. The surface profiles of the three topographically distinct films are shown in Figure 3a. All the films possessed a fine degree of porosity, which is presumed to have resulted from the local pockets of phase segregation and the entrapment of air bubbles entailed by it. Spin-casting films on PDMS templates did not manage to eliminate this porosity. Its role may be important considering the intended utilization of these films for the release of antibiotics either in the treatment of osteomyelitis or in the prophylaxis against implant-related infections, whereby a finite level of burst release caused by these pores is thought to be a desirable feature.

3.2. Model Drug Release. Indeed, the release profile for a small molecule, fluorescein, from PCL/HAp films, shown in Figure 5, demonstrated a finite amount of burst release occurring in the first hour following the immersion of the films into the solution, though accounting for only ~10% of the entire drug load. The release pattern then entered its second phase when the release stabilized at ~0.6 μg/h. In theory, if the same drug release profile in this stage applied to an antibiotic molecule of a similar size and diffusion coefficient, such as clindamycin, gentamicin or tobramycin, the minimal inhibitory concentration would be exceeded for most bacteria in the immediate vicinity of the implanted film. Unlike pure HAp, typified by the initial burst release of the adsorbed drug and the rather insubstantial release in the subsequent, sustained release
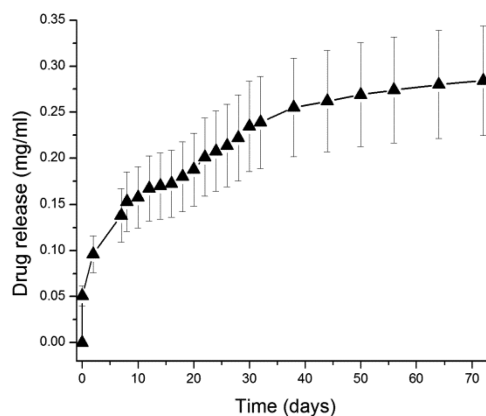

Figure 5. Temporal profile for the sustained release of fluorescein from PCL/HAp films in PBS.

phase, PCL has been used to ensure extended release profiles both alone[49,50] and in composites.[51,52] Owing to its comparatively long hydrocarbon chains and the resulting hydrophobicity, PCL is one of the slowest degrading poly(α-hydroxy esters), needing several years to undergo complete degradation at the molecular weight of 80 kDa.[53] Consequently, only $48 \pm 4\%$ of the model drug was released from the films after 2.5 months of incubation in an unstirred physiological solution. At the rate of release observed toward the end of the incubation time, it would take approximately 7 more months for the entire load to be released from the composite films. However, degradation and drug release from polymeric and other implants in vivo are typically higher than in vitro.[54,55] One of the contributing factors would, in this case, be the hydrolytic action of proteases, which have been shown to be able to fully degrade PCL implants in vitro in only 1 month or so.[56] Another contributing factor might be the possibly higher degradation rate of PCL at acidic pHs,[57] the conditions under which osteoclasts degrade boney tissues. Phagocytosis, biomechanical stress and increased wetting in biological conditions can present other factors that may lead to higher degradability of the given composites in vivo.[58,59] The thickness of PCL/HAp films is a parameter that has not been systematically investigated in this study and that could be increased to more than 100 μm to additionally extend the drug release time window.

3.3. Phenotypic Response of the Osteoblastic Cells. The initial proliferation of fibroblasts on PCL/HAp films, 4 days after the seeding, was hampered compared to their proliferation on the control polystyrene surface (Figure 6a). The number of cells at this early time point was thus 37.5% of the control on the periodically arranged PCL/HAp films, 61% on the irregularly textured ones and 68% on the flat ones. After the growth times ranging from 7 to 10 days, however, the cell number on PCL/HAp substrates was restored in comparison with the control and no significant difference in cell number was found. The morphologies of cells counterstained at this point against collagen type I and nucleus appeared healthy and well spread across the underlying surface (Figure 7). Equally solid production of collagen among the entire cell population served as an evidence of the cells' uncompromised ability to form extracellular matrix following growth on PCL/HAp films. Interestingly, after 12 days of growth, the number of cells on all PCL/HAp films was higher than on the control plastic. In contrast, no consistently significant decrease in the mitochon-
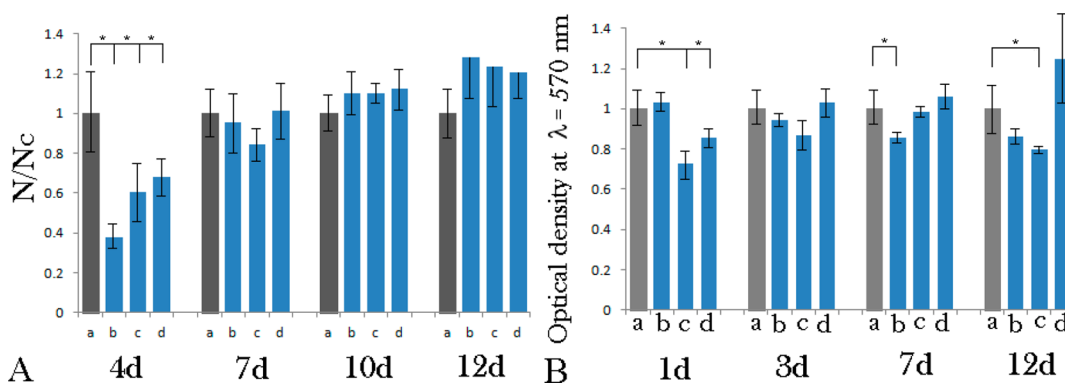
Figure 6. (A) Proliferation of MC3T3-E1 cells after 4, 7, 10 and 12 days of incubation on different PCL/HAp films, (b) topographically ordered, (c) topographically disordered and (d) flat, normalized to proliferation on control cell culture polystyrene (a). The proliferation ratio is represented as a number of cells counted per surface area for a given sample (N) normalized to the number of cells per surface area for the control sample (N_c). (B) MTT viability assay for MC3T3-E1 cells on control cell culture polystyrene (a) and on different PCL/HAp films, (b) topographically ordered, (c) topographically disordered and (d) flat, after 1, 3, 7 and 12 days of incubation. Samples for which a statistically significant difference ($p < 0.05$) was observed when compared to the control are denoted with *.
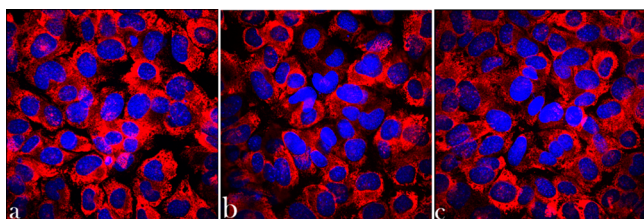

Figure 7. Volume-rendered confocal optical micrographs of osteoblastic MC3T3-E1 cells grown for 7 days on various PCL/HAp substrates and fluorescently stained for collagen type I (red) and nucleus (blue): (a) topographically ordered, (b) topographically disordered and (c) flat.

drial activity of cells, directly indicative of their viability, was detected following their growth on PCL/HAp films for any period of time between 1 and 12 days (Figure 6b).

Figure 8 demonstrates that the migration of MC3T3-E1 fibroblasts onto PCL/HAp films proceeded slower than on the control borosilicate glass. The flat composite films, however, fostered more cell migration activity than the films containing
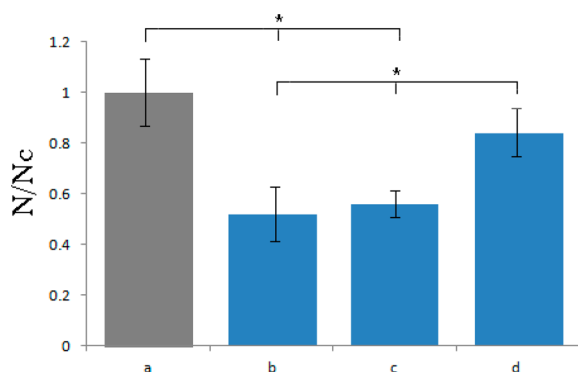

Figure 8. Migration assay for MC3T3-E1 cells onto control cell culture borosilicate glass (a) and onto different PCL/HAp films, (b) topographically ordered, (c) topographically disordered and (d) flat, after 3 days of incubation. Migration density is represented as a number of cells counted per surface area for a given sample (N) normalized to the number of cells per surface area for the control sample (N_c). Statistically significant difference ($p < 0.05$) is denoted with *.

topographic features. The fact that the migration of fibroblasts onto PCL/HAp films was slower than onto the control glass surface might have certain therapeutic repercussions, given that the bone substitute implantation presents the onset of the above-mentioned "race for the surface" involving bone cells and opportunistic bacteria, with its winner often determining the success of the therapeutic outcome. Compared to the flat PCL/HAp films, the microtextured ones led to slower cell migration onto them, illustrating the ability of the surface features to hinder cell movement. This ability, however, has its potential positive effects too, as in theory, it may favor a more intimate material/tissue interface, especially because it is known that adhesion antecedes osteogenesis.[60] Provided that the cells succeed in adhering to the topographically enriched substrate, it can be expected that a lesser mobility of the adherent soft tissue and its tighter adherence to the implant may result.[61]

3.4. Genotypic Response of the Osteoblastic Cells. The lower proliferation of cells seeded on the topographically symmetrical PCL/HAp substrates coincided with the lowest expression of the housekeeping gene, β-actin, in cells grown on these very same surfaces. Similar to what was seen with proliferation and migration assays, cells grown on the topographically asymmetrical PCL/HAp substrates had higher levels of β-actin, but not as much as those grown on the flat PCL/HAp surfaces, let alone on the control tissue culture polystyrene. The fact that the absolute β-actin expression trend was identical to that of the proliferation assay (Figure 8) implied that the expression of this housekeeping gene could be used as a valid normalization factor in assessing the expression of osteogenic marker genes. In contrast with the results of proliferation and migration assays, the gene expression data demonstrate that the osteogenic activity was significantly increased for the cells grown on PCL/HAp films comprising topographically ordered features compared to both the control polystyrene surface and two other types of PCL/HAp films analyzed (Figure 9). Table 2 lists the main osteogenesis-related functions of the proteins encoded by genes analyzed for mRNA expression. From osteocalcin, a least ambiguous osteogenic marker, whose upregulation practically always correlates with an increase in the bone density, to alkaline phosphatase, a protein involved in numerous biological processes and present in virtually all tissues, the expression of all the analyzed genes was increased typically multifold with respect to the control
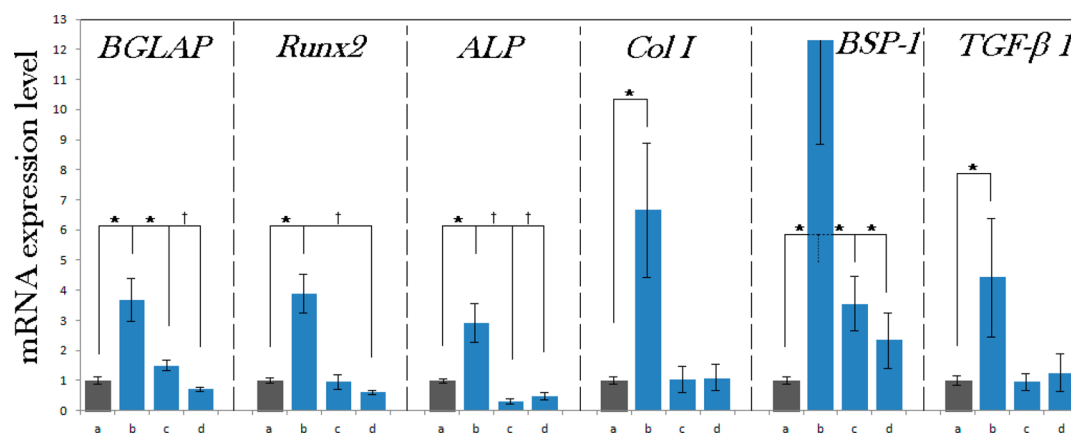
13215

dx.doi.org/10.1021/am503043t | ACS Appl. Mater. Interfaces 2014, 6, 13209–13220

Figure 9. Normalized mRNA expression of six different osteogenic markers in MC3T3-E1 cells grown on control cell culture polystyrene (a) and on different PCL/HAp films, (b) topographically ordered, (c) topographically disordered and (d) flat, after 96 h of incubation. mRNA expression was detected by quantitative RT-polymerase chain reaction relative to the housekeeping gene β-actin (*ACTB*). Data normalized to the expression of *ACTB* are shown as averages with error bars representing standard deviation. Genes significantly ($p < 0.05$) upregulated with respect to the control group are marked with *. Genes significantly ($p < 0.05$) downregulated with respect to the control group are marked with [†].

Table 2. Genes Analyzed for mRNA Expression Using qPCR, the Proteins They Encode for and Their Main Biological Function during Osteogenesis

gene	protein name	main role during osteogenesis
BGLAP	osteocalcin	promoter of mineral nucleation[62,63]
Runx2	runt-related transcription factor 2	mesenchymal precursor for cell differentiation into osteoblastic lineage[64,65]
ALP	alkaline phosphatase	dephosphorylation enzyme and a byproduct of osteoblastic activity[66]
Col I	procollagen type I	precursor of collagen type I, the main organic phase of boney tissues[67]
BSP-1	osteopontin	mineral nucleation inhibitor and the functional antagonist of osteocalcin[68]
TGFβ-1	transforming growth factor β-1	antagonist of bone morphogenetic proteins in the canonical Smad-dependent signaling pathways[69] and osseointegration stimulant[70]
ACTB	β-actin	cytoskeletal microfilament regulating motility and structural integrity of the cell[71]

sample as well as to the cells grown on flat or topographically randomized PCL/HAp substrates. In contrast, no consistently significant increase in the expression of any of the seven osteogenic markers was detected for the flat PCL/HAp films when compared to the control polystyrene. These observations support the notion that topography can be a far more important determinant of the cell/surface interaction than the surface chemistry, stiffness and ζ-potential. Moreover, the fact that the osteogenic activity was markedly more stimulated on the topographically ordered PCL/HAp films compared to topographically disordered films of the same composition implies that the regularity of the distribution of topographic features can be a more important variable than the topographic features per se and an essential one to consider in the design of biomaterials.

Perhaps the cause of this elevated expression of osteogenic markers in cells seeded on polymer—ceramic composite substrates with topographies exhibiting high levels of translational symmetry can be correlated with the largest amount of mechanical stress imposed on the cells by them. Namely, as can be seen from Figure 7a, after 96 h of incubation, which is the same time range in which the real-time PCR data shown in Figure 9 were collected, the cell number was significantly lower on PCL/HAp surfaces than on the polystyrene control, before

it caught up at longer incubation times ($\geq$7 days). Proliferation is typically hindered at the onset of cell differentiation and, consequently, its drop was directly suggestive of the ability of the topographically ordered PCL/HAp substrates to accelerate the differentiation of fibroblastic MC3T3-E1 cells into an osteoblastic lineage. Previous studies have concordantly demonstrated that preosteoblastic cells do exit the proliferation phase and enter the osteogenic differentiation phase earlier when grown of microrough surfaces than when they are seeded on smooth surfaces.[72] Also, the absolute expression of β-actin followed the same trend as for proliferation, being the highest for the control polystyrene and the lowest for the topographically ordered PCL/HAp films. β-actin is a housekeeping gene and its expression correlates well with the cell number and can be therefore used as another optional proliferation marker. Additionally, both proliferation and β-actin expression were significantly higher for cells grown on flat PCL/HAp films than on any of the textured ones, serving as an evidence for the stressful effect of topographic features on the cell growth when the dimensions of the two are in the same range, as it happened to be inherent in the design of this study (Figure 4). Even cells grown on disarrayed PCL/HAp films initially proliferated better and expressed β-actin more abundantly than the ordered ones, the reason presumably being more sufficient spacing between the surface features, allowing for more facile settling of the cells in-between them. Imposition of a moderate mechanochemical stress onto osteoblasts by the bone replacement materials may thus be an inescapable route for producing conditions of higher osteogenic activity and increasing the bone regeneration potential of their application.

3.5. Correlation with the Essentiality of Inflammation for Bone Regeneration. The deduced idea that the imposition of an optimal mechanochemical stress onto osteoblasts increases their regenerative capacity is tied to the common misconception that inflammation is undesirable in tissue regeneration as it interferes adversely with the healing process. Rather, by attracting leukocytes and macrophages to the implantation site and stimulating angiogenesis, moderate inflammation promotes tissue regeneration. On one hand, this helps in swelling the biodegradable polymeric implants, speeding up their degradation via hydrolysis, while on the other hand, it induces a signaling cascade that results in the

production of cytokines and differentiation of monocytes into osteoclasts,[73] the cells that would, together with phagocytes, go on to resorb the organic and biodegradable ceramic implants. Inflammation paralleled with the increased concentration of lymphocytes has also been shown to promote the proliferation and differentiation of MSCs, the cells capable of migrating to the sites of inflammation or injury to partake in their healing.[74] Delayed inflammatory response to injury thus usually directly translates to impaired tissue regeneration.[75] The fact that Si- and Sr-doped calcium phosphate implants are more smoothly taken up by the body than the pure compounds[76,77] could potentially be explained by the ability of these two foreign ions to trigger a mild immunological alarm, which would produce just enough of the inflammatory response to ensure the resorption of the implant and the formation of new bone at its place in the stead of inert encapsulation. To further bone regeneration, some of the traditional reparative techniques in orthopedics have thus directly prescribed an infliction of injury or infection, as in the case when short bones are fractured by the physicians to induce their elongation or when swabs contaminated with staphylococci are applied to an open bone following a surgery performed on it so as to speed up its recovery. Similarly, for gene transfection to be effectively performed, required is a carrier that exhibits moderate levels of cytotoxicity, able to rupture and penetrate the cell membrane prior to releasing the therapeutic agent targeting the nucleus. Moreover, it was shown that activation of inflammatory pathways is favorable for the purpose of a successful gene therapy in a sense that it opens chromatin and allows for the genetic information to be interfered with, which has led to the coinage of the term "transflammation" to more veritably describe the process of gene transfection.[78] Regeneration and inflammation signaling pathways in the cell are, in fact, tightly entwined, and stimulating one may not be possible without stimulation of the other. This can be exemplified by a number of proinflammatory molecular mediators that act as essential components of regeneration pathways within the cell.[79] The activation of proinflammatory cytokines is thus a prerequisite for proper bone healing to occur,[79] leading to an inextricable entwinement of injury and repair in the clinical context. By analogy, we could conclude that drug delivery devices and tissue regeneration materials may need to be optimally injurious to the body in order to achieve a maximal therapeutic effect.

3.6. Need for Surface Feature Optimization at Both Micro and Nano Scales. Hereby we demonstrate the greatest level of osteoblastic activity induced in cells grown on PCL/HAp surfaces comprising periodically arranged topographic features, as opposed to the control polystyrene, flat PCL/HAp films or PCL/HAp films with identical but randomized surface features. In a former study by Dalby et al., the opposite was found: namely, randomly patterned poly(methyl methacrylate) substrates, though with nanosized, not microsized features, substituted for the role of osteogenic supplements and induced the differentiation of MSCs to osteoblasts, unlike the chemically identical substrates with a perfect translational symmetry.[80] The different outcomes of these two studies may have been caused by the different cell types used (MSCs vs MC3T3-E1), by the different compounds used to grow the cells on (poly(methyl methacrylate) vs PCL/HAp), or perhaps by the 2 orders of magnitude lower size scale of the features utilized (120 nm in diameter, 300 in spacing and 100 nm in depth vs 10 μm in diameter, 20 μm in separation and 10 μm in height). Different effects accomplished by the topographic

features on the micro scale and on the nano scale suggest that tailoring of the surface of a biomaterial for a most favorable interface with the adjacent tissue should be done at both scales. Perhaps neither of the topographies outweighs in its importance the other one. The precisely defined topographic spacing at the nano scale, such as the 40 nm wide gap and the 27 nm wide overlap region of collagen fibers, can be sensed by the cells and even the finest changes on this length scale can have a relatively large effect on cell adherence and proliferation.[81] On the other hand, here we show that, in analogy with the world of optics, characteristics of the surface features comparable in size with the cells seeded on them can have a similarly drastic effect on their growth. Moreover, our earlier study showed that calcium phosphate nanoparticles augment proliferation and the osteogenic response of osteoblastic cells to a greater extent than the microsized particles do.[82] In this work, however, we demonstrate that the choice of the right features at the micro scale could be used to impose moderate mechanochemical stress on the adherent cells and thus boost their osteogenic activity.

4. SUMMARY

Both sole bottom-up and top-down techniques for the synthesis of nanostructures suffer from inherent weaknesses. As for the former, they include difficult integration of the products into devices, whereas the downsides of the latter include expensive processing and robust equipment that deters the easy transfer of technologies.[83] Enforcing either one or the other approach to the fabrication of nanostructures can be blamed for the fact that nanomaterials, not nanodevices, still comprise the major share of patents in the field of nanotechnologies as well as that the global market for nanotechnologies was, in 2009, only 1.1% of its value predicted by the National Science Foundation five years earlier.[84] It has been hypothesized therefore that various combinations of the two may hold the greatest prospect in advanced materials synthesis.[85,86] As a proof of principle, composite films comprising PCL and HAp were fabricated in this study using a combination of bottom-up, wet, precipitation synthesis of the nanoparticulate phase, in this case HAp, and top-down, photolithographic imprinting of precisely designed topographic features. The films were able to capture a considerable amount of small model drug molecules and release it over extended periods of time. Their performance in vitro, as a substrate for the growth of the fibroblastic and/or osteoblastic MC3T3-E1 cell line, was evaluated. The greatest level of mechanochemical stress was, however, imposed on cells by the PCL/HAp films with regularly distributed surface features and this elevated stress directly translated to osteogenic activity higher than (a) on flat PCL/HAp films, (b) on PCL/HAp films comprising randomly distributed features and (c) on the control tissue culture polystyrene. It was thus shown that topography can be a more important determinant of the cell/surface interaction than the surface chemistry and/or stiffness as well as that the regularity of the distribution of topographic features can be a more important variable than the topographic features per se. The broad conclusion of the study is that the precise tailoring of the surface of artificial bone substitutes and biomaterials in general for the most favorable material/cell interaction has to take into account both the dimensions of the surface features and the level of their translational symmetry.

■ AUTHOR INFORMATION

Corresponding Authors

*V. Uskoković. E-mail: uskok@uic.edu.
*T. A. Desai. E-mail: tejal.desai@ucsf.edu.

Notes

The authors declare no competing financial interest.

■ REFERENCES

(1) Gristina, A. G. Biomaterial-Centered Infection: Microbial Adhesion versus Tissue Integration. *Science* **1987**, *237*, 1588−1595.

(2) Gu, Y. X.; Du, J.; Si, M. S.; Mo, J. J.; Qiao, S. C.; Lai, H. C. The Roles of PI3K/Akt Signaling Pathway in Regulating MC3T3-E1 Preosteoblast Proliferation and Differentiation on SLA and SLActive Titanium Surfaces. *J. Biomed. Mater. Res., Part A* **2013**, *101*, 748−754.

(3) Zamani, F.; Amani-Tehran, M.; Latifi, M.; Shokrgozar, M. A. The Influence of Surface Nanoroughness of Electrospun PLGA Nanofibrous Scaffold on Nerve Cell Adhesion and Proliferation. *J. Mater. Sci.: Mater. Med.* **2013**, *24*, 1551−1560.

(4) Teng, N. C.; Wang, P. D.; Chang, W. J.; Feng, S. W.; Fan, K. H.; Lin, C. T.; Hsieh, S. C.; Huang, H. M. Er:YAG Laser-Roughened Enamel Promotes Osteoblastic Differentiation. *Photomed. Laser Surg.* **2012**, *30*, 516−522.

(5) Müller, B. Tailoring Biocompatibility: Benefitting Patients. *Mater. Today* **2010**, *13*, 58.

(6) Schwartz, Z.; Raz, P.; Zhao, G.; Barak, Y.; Tauber, M.; Yao, H.; Boyan, B. D. Effect of Micrometer-Scale Roughness of the Surface of Ti6Al4V Pedicle Screws in Vitro and in Vivo. *J. Bone Jt. Surg., Am. Vol.* **2008**, *90*, 2485−2498.

(7) Mamalis, A.; Silvestros, S. Modified Titanium Surfaces Alter Osteogenic Differentiation: A Comparative Microarray-Based Analysis of Human Mesenchymal Cell Response to Commercial Titanium Surfaces. *J. Oral Implantol.* **2013**, *39*, 591−601.

(8) Wennerberg, A.; Albrektsson, T. Effects of Titanium Surface Topography on Bone Integration: A Systematic Review. *Clin. Oral. Implants Res.* **2009**, *20*, 172−84.

(9) Wittenburg, G.; Lauer, G.; Oswald, S.; Labudde, D.; Franz, C. M. Nanoscale Topographic Changes on Sterilized Glass Surfaces Affect Cell Adhesion and Spreading. *J. Biomed. Mater. Res., Part A* **2014**, *102*, 2755−2766.

(10) Guo, J.; Morris, J. R.; Ihm, Y.; Contescu, C. I.; Gallego, N. C.; Duscher, G.; Pennycook, S. J.; Chisholm, M. F. Topological Defects: Origin of Nanopores and Enhanced Adsorption Performance in Nanoporous Carbon. *Small* **2012**, *8*, 3283−3288.

(11) Guczi, L.; Horvath, D.; Paszti, Z.; Peto, G. Effect of Treatments on Gold Nanoparticles: Relation between Morphology, Electron Structure and Catalytic Activity in CO Oxidation. *Catal. Today* **2002**, *72*, 101−105.

(12) Czoschke, P.; Hong, H.; Basile, L.; Chiang, T.-C. Quantum Beating Patterns in the Energetics of Thin Film Nanostructures. *Phys. Rev. Lett.* **2003**, *91*, 226801.

(13) Ito, H.; Sasaki, H.; Saito, K.; Honma, S.; Yajima, Y.; Yoshinari, M. Response of Osteoblast-Like Cells to Zirconia with Different Surface Topography. *Dent. Mater. J.* **2013**, *32*, 122−129.

(14) Altmann, B.; Kohal, R. J.; Steinberg, T.; Tomakidi, P.; Bächle-Haas, M.; Wennerberg, A.; Att, W. Distinct Cell Functions of Osteoblasts on UV-Functionalized Titanium- and Zirconia-Based Implant Materials are Modulated by Surface Topography. *Tissue Eng., Part C* **2013**, *19*, 850−863.

(15) Olivares-Navarrete, R.; Hyzy, S. L.; Gittens, R. A.; Schneider, J. M.; Haithcock, D. A.; Ullrich, P. F.; Slosar, P. J.; Schwartz, Z.; Boyan, B. D. Rough Titanium Alloys Regulate Osteoblast Production of Angiogenic Factors. *Spine J.* **2013**, *13*, 1563−1570.

(16) Kohal, R. J.; Bächle, M.; Att, W.; Chaar, S.; Altmann, B.; Renz, A.; Butz, F. Osteoblast and Bone Tissue Response to Surface Modified Zirconia and Titanium Implant Materials. *Dent. Mater.* **2013**, *29*, 763−776.

(17) Webster, T. J.; Ergun, C.; Doremus, R. H.; Siegel, R. W.; Bizios, R. Enhanced Functions of Osteoblasts on Nanophase Ceramics. *Biomaterials* **2000**, *21*, 1803−1810.

(18) Wilkinson, A.; Hewitt, R. N.; McNamara, L. E.; McCloy, D.; Meek, R. M. D.; Dalby, M. J. Biomimetic Microtopography to Enhance Osteogenesis *in vitro*. *Acta Biomat.* **2011**, *7*, 2919−2925.

(19) Lamers, E.; Walboomers, X. F.; Domanski, M.; te Riet, J.; van Delft, F. C.; Luttge, R.; Winnubst, L. A.; Gardeniers, H. J.; Jansen, J. A. The Influence of Nanoscale Grooved Substrates on Osteoblast Behavior and Extracellular Matrix Deposition. *Biomaterials* **2010**, *31*, 3307−3316.

(20) Wang, P. Y.; Li, W. T.; Yu, J.; Tsai, W. B. Modulation of Osteogenic, Adipogenic and Myogenic Differentiation of Mesenchymal Stem Cells by Submicron Grooved Topography. *J. Mater. Sci. Mater. Med.* **2012**, *23*, 3015−3028.

(21) Mozumder, M. S.; Zhu, J.; Perinpanayagam, H. Titania-Polymeric Powder Coatings with Nano-Topography Support Enhanced Human Mesenchymal Cell Responses. *J. Biomed. Mater. Res., Part A* **2012**, *100*, 2695−2709.

(22) Ahn, E. H.; Kim, Y.; Kshitiz, A. S. S.; Afzal, J.; Lee, S.; Kwak, M.; Suh, K. Y.; Kim, D. H.; Levchenko, A. Spatial Control of Adult Stem Cell Fate Using Nanotopographic Cues. *Biomaterials* **2014**, *35*, 2401−2410.

(23) Zink, C.; Hall, H.; Brunette, D. M.; Spencer, N. D. Orthogonal Nanometer-Micrometer Roughness Gradients Probe Morphological Influences on Cell Behavior. *Biomaterials* **2012**, *33*, 8055−8061.

(24) Uskoković, V.; Desai, T. A. Phase Composition Control of Calcium Phosphate Nanoparticles for Tunable Drug Delivery Kinetics and Treatment of Osteomyelitis. Part 1: Preparation and Drug Release. *J. Biomed. Mater. Res., Part A* **2013**, *101*, 1416−1426.

(25) Hilbrig, F.; Freitag, R. Hydroxyapatite in bioprocessing. In *Biopharmaceutical production technology*, Vol. 1; Subramanian, G, Ed.; Wiley-VCH: Weinheim, Germany, 2012; pp 283−331.

(26) Do, T. N.; Lee, W. H.; Loo, C. Y.; Zavgorodniy, A. V.; Rohanizadeh, R. Hydroxyapatite Nanoparticles As Vectors for Gene Delivery. *Ther. Delivery* **2012**, *3*, 623−632.

(27) Lin, L.; Chow, K. L.; Leng, Y. Study of Hydroxyapatite Osteoinductivity with an Osteogenic Differentiation of Mesenchymal Stem Cells. *J. Biomed. Mater. Res., Part A* **2009**, *89*, 326−335.

(28) Uskoković, V.; Desai, T. A. Phase Composition Control of Calcium Phosphate Nanoparticles for Tunable Drug Delivery Kinetics and Treatment of Osteomyelitis. Part 2: Antibacterial and Osteoblastic Response. *J. Biomed. Mater. Res., Part A* **2013**, *101*, 1427−1436.

(29) Causa, F.; Netti, P. A.; Ambrosio, L.; Ciapetti, G.; Baldini, N.; Pagani, S.; Martini, D.; Giunti, A. Poly-Epsilon-Caprolactone/Hydroxyapatite Composites for Bone Regeneration: In Vitro Characterization and Human Osteoblast Response. *J. Biomed. Mater. Res., Part A* **2006**, *76*, 151−162.

(30) Kim, H. W.; Knowles, J. C.; Kim, H. E. Hydroxyapatite/Poly(Epsilon-Caprolactone) Composite Coatings on Hydroxyapatite Porous Bone Scaffold for Drug Delivery. *Biomaterials* **2004**, *25*, 1279−87.

(31) Shokrollahi, P.; Mehmanchi, M.; Atai, M.; Omidian, H.; Shokrolahi, F. Effect of Interface on Mechanical Properties and Biodegradation of PCL HAp Supramolecular Nano-Composites. *J. Mater. Sci.: Mater. Med.* **2014**, *25*, 23−35.

(32) Uskoković, V.; Desai, T. A. *In Vitro* Analysis of Nanoparticulate Hydroxyapatite/Chitosan Composites as Potential Drug Delivery Platforms for the Sustained Release of Antibiotics in the Treatment of Osteomyelitis. *J. Pharm. Sci.* **2014**, *103*, 567−579.

(33) Vukomanović, M.; Škapin, S.; Jančar, B.; Maksin, T.; Ignjatović, N.; Uskoković, V.; Uskoković, D. Poly(D,L-Lactide-co-Glycolide)/ Hydroxyapatite Core-Shell Nanospheres. Part 1: A Multifunctional System for Controlled Drug Delivery. *Colloids Surf., B* **2011**, *82*, 404− 413.

(34) Siparsky, G. L.; Voorhees, K. J.; Miao, F. Hydrolysis of Polylactic Acid (PLA) and Polycaprolactone (PCL) in Aqueous Acetonitrile Solutions: Autocatalysis. *J. Environ. Polym. Degrad.* **1998**, *6*, 31−41.

(35) Bostman, O. M. Osteotic Changes Accompanying Degradation of Absorbable Fracture Fixation Implants. *J. Bone Jt. Surg., Br. Vol.* **1991**, *73*, 679−682.

(36) Uskoković, V.; Uskoković, D. P. Nanosized Hydroxyapatite and Other Calcium Phosphates: Chemistry of Formation and Application as Drug and Gene Delivery Agents. *J. Biomed. Mater. Res., Part B* **2011**, *96*, 152−191.

(37) Martínez, E.; Engel, E.; López-Iglesias, C.; Mills, C. A.; Planell, J. A.; Samitier, J. Focused Ion Beam/Scanning Electron Microscopy Characterization of Cell Behavior on Polymer Micro-/Nanopatterned Substrates: A Study of Cell-Substrate Interactions. *Micron* **2008**, *39*, 111−116.

(38) Charest, J. L.; Eliason, M. T.; García, A. J.; King, W. P. Combined Microscale Mechanical Topography and Chemical Patterns on Polymer Cell Culture Substrates. *Biomaterials* **2006**, *27*, 2487− 2494.

(39) Zapata, P.; Su, J.; García, A. J.; Meredith, J. C. Quantitative High-Throughput Screening of Osteoblast Attachment, Spreading, and Proliferation on Demixed Polymer Blend Micropatterns. *Biomacromolecules* **2007**, *8*, 1907−1917.

(40) Gu, Y.; Chen, X.; Lee, J. H.; Monteiro, D. A.; Wang, H.; Lee, W. Y. Inkjet Printed Antibiotic- and Calcium-Eluting Bioresorbable Nanocomposite Micropatterns for Orthopedic Implants. *Acta Biomater.* **2012**, *8*, 424−431.

(41) Uskoković, V. Nanotechnologies: What We Do Not Know. *Technol. Soc.* **2007**, *29*, 43−61.

(42) Bittiger, H.; Marchessault, R. H.; Niegisch, W. D. Crystal Structure of Poly-ε-Caprolactone. *Acta Crystallogr., Sect. B: Struct. Crystallogr. Cryst. Chem.* **1970**, *26*, 1923−1932.

(43) Baji, A.; Wong, S.-C.; Liu, T.; Li, T.; Srivatsan, T. S. Morphological and X-ray Diffraction Studies of Crystalline Hydroxyapatite-Reinforced Polycaprolactone. *J. Biomed. Mater. Res., Part B* **2006**, *81*, 343−350.

(44) Xiao, X.; Liu, R.; Huang, Q.; Ding, X. Preparation and Characterization of Hydroxyapatite/Polycaprolactone-Chitosan Composites. *J. Mater. Sci. Mater. Med.* **2009**, *20*, 2375−2383.

(45) Lam, C. X.; Hutmacher, D. W.; Schantz, J. T.; Woodruff, M. A.; Teoh, S. H. Evaluation of Polycaprolactone Scaffold Degradation for 6 Months in Vitro and in Vivo. *J. Biomed. Mater. Res., Part A* **2009**, *90*, 906−919.

(46) Takagi, S.; Frukhtbeyn, S.; Chow, L. C.; Sugawara, A.; Fujikawa, K.; Ogata, H.; Hayashi, M.; Ogiso, B. In Vitro and in Vivo Characteristics of Fluorapatite-Forming Calcium Phosphate Cements. *J. Res. Natl. Inst. Stand. Technol.* **2010**, *115*, 267−276.

(47) Linhart, W.; Briem, D.; Amling, M.; Rueger, J. M.; Windolf, J. Mechanical Failure of Porous Hydroxyapatite Ceramics 7.5 Years after Implantation in the Proximal Tibial. *Unfallchirurg* **2004**, *107*, 154− 157.

(48) Xia, L.; Lin, K.; Jiang, X.; Fang, B.; Xu, Y.; Liu, J.; Zeng, D.; Zhang, M.; Zhang, X.; Chang, J.; Zhang, Z. Effect of Nano-Structured Bioceramic Surface on Osteogenic Differentiation of Adipose Derived Stem Cells. *Biomaterials* **2014**, DOI: 10.1016/j.biomaterials.2014.06.028, in press.

(49) Bernards, D. A.; Lance, K. D.; Ciaccio, N. A.; Desai, T. A. Nanostructured Thin Film Polymer Devices for Constant-Rate Protein Delivery. *Nano Lett.* **2012**, *12*, 5355−5361.

(50) Chang, H. I.; Williamson, M. R.; Perrie, Y.; Coombes, A. G. Precipitation Casting of Drug-Loaded Microporous PCL Matrices: Incorporation of Progesterone by Co-Dissolution. *J. Controlled Release* **2005**, *106*, 263−272.

(51) Fang, T.; Wen, J.; Zhou, J.; Shao, Z.; Dong, J. Poly(ε-Caprolactone) Coating Delays Vancomycin Delivery from Porous Chitosan/β-Tricalcium Phosphate Composites. *J. Biomed. Mater. Res., Part B* **2012**, *100*, 1803−1811.

(52) Zalfen, A. M.; Nizet, D.; Jérôme, C.; Jérôme, R.; Frankenne, F.; Foidart, J. M.; Maquet, V.; Lecomte, F.; Hubert, P.; Evrard, B. Controlled Release of Drugs From Multi-Component Biomaterials. *Acta Biomater.* **2008**, *4*, 1788−1796.

(53) Cameron, R. E.; Kamvari-Moghaddam, A. Synthetic Bioresorbable Polymers. In *Degradation Rate of Bioresorbable Materials*; Buchanan, F., Ed.; Woodhead: Cambridge, U. K., 2008; pp 43−66.

(54) Oh, S. H.; Kang, S. G.; Lee, J. H. Degradation Behaviour of Hydrophilized PLGA Scaffolds Prepared by Melt-Moulding Particulate-Leaching Method: Comparison with Control Hydrophobic One. *J. Mater. Sci.: Mater. Med.* **2006**, *17*, 131−137.

(55) Bansal, S. S.; Vadhanam, M. V.; Gupta, R. C. Development and in Vitro-in Vivo Evaluation of Polymeric Implants for Continuous Systemic Delivery of Curcumin. *Pharm. Res.* **2011**, *28*, 1121−1130.

(56) Peng, H.; Ling, J.; Liu, J.; Zhu, N.; Ni, X.; Shen, Z. Controlled Enzymatic Degradation of Poly(ε-caprolactone)-Based Copolymers in the Presence of Porcine Pancreatic Lipase. *Polym. Degrad. Stab.* **2010**, *95*, 643−650.

(57) Coffin, M. D.; McGinity, J. W. Biodegradable Pseudolatexes: The Chemical Stability of Poly(D,L-Lactide) and Poly(ε-Caprolactone) Nanoparticles in Aqueous Media. *Pharm. Res.* **1992**, *9*, 200−205.

(58) Tomlins, P. Influence of Porous Structure on Bioresorbability: Tissue Engineering Scaffolds. In *Degradation Rate of Bioresorbable Materials*; Buchanan, F., Ed.; Woodhead: Cambridge, U. K., 2008; pp 234−264.

(59) Claes, L. E. Mechanical Characterization of Biodegradable Implants. *Clin. Mater.* **1992**, *10*, 41−46.

(60) Kilian, K. A.; Bugarija, B.; Lahn, B. T.; Mrksich, M. Geometric Cues for Directing the Differentiation of Mesenchymal Stem Cells. *Proc. Natl. Acad. Sci. U. S. A.* **2010**, *107*, 4872−4877.

(61) Parker, J. A.; Walboomers, X. F.; Von den Hoff, J. W.; Maltha, J. C.; Jansen, J. A. The Effect of Bone Anchoring and Micro-Grooves on the Soft Tissue Reaction to Implants. *Biomaterials* **2002**, *23*, 3887− 3896.

(62) Lian, J. B.; Stein, G. S.; Stein, J. L.; van Wijnen, A. J. Osteocalcin Gene Promoter: Unlocking the Secrets for Regulation of Osteoblast Growth and Differentiation. *J. Cell Biochem. Suppl.* **1998**, *30−31*, 62− 72.

(63) Neve, A.; Corrado, A.; Cantatore, F. P. Osteocalcin: Skeletal and Extra-Skeletal Effects. *J. Cell Physiol.* **2013**, *228*, 1149−1153.

(64) Carbonare, L. D.; Innamorati, G.; Valenti, M. T. Transcription Factor Runx2 and its Application to Bone Tissue Engineering. *Stem Cell Rev.* **2012**, *8*, 891−897.

(65) Komori, T. Signaling Networks in RUNX2-Dependent Bone Development. *J. Cell Biochem.* **2011**, *112*, 750−755.

(66) Pagani, F.; Francucci, C. M.; Moro, L. Markers of Bone Turnover: Biochemical and Clinical Perspectives. *J. Endocrinol. Invest.* **2005**, *28*, 8−13.

(67) Christenson, R. H. Biochemical Markers of Bone Metabolism: An Overview. *Clin. Biochem.* **1997**, *30*, 573−593.

(68) Sodek, J.; Ganss, B.; McKee, M. D. Osteopontin. *Crit. Rev. Oral Biol. Med.* **2000**, *11*, 279−303.

(69) Chen, G.; Deng, C.; Li, Y. P. TGF-β and BMP Signaling in Osteoblast Differentiation and Bone Formation. *Int. J. Biol. Sci.* **2012**, *8*, 272−288.

(70) Lamberg, A.; Schmidmaier, G.; Søballe, K.; Elmengaard, B. Locally Delivered TGF-Beta1 and IGF-1 Enhance the Fixation of Titanium Implants: A Study in Dogs. *Acta Orthop.* **2006**, *77*, 799−805.

13219

dx.doi.org/10.1021/am503043t | *ACS Appl. Mater. Interfaces* 2014, 6, 13209−13220

(71) Lin, J.; Redies, C. Histological Evidence: Housekeeping Genes Beta-Actin and GAPDH are of Limited Value for Normalization of Gene Expression. *Dev. Genes Evol.* **2012**, *222*, 369−376.

(72) Gittens, R. A.; Olivares-Navarrete, R.; Schwartz, Z.; Boyan, B. D. Implant Osseointegration and the Role of Microroughness and Nanostructures: Lessons for Spine Implants. *Acta Biomater.* **2014**, *10*, 3363−3371.

(73) Narducci, P.; Nicolin, V. Differentiation of Activated Monocytes into Osteoclast-Like Cells on a Hydroxyapatite Substrate: An in Vitro Study. *Ann. Anat.* **2009**, *191*, 349−355.

(74) Wu, X.; Wang, W.; Meng, C.; Yang, S.; Duan, D.; Xu, W.; Liu, X.; Tang, M.; Wang, H. Regulation of Differentiation in Trabecular Bone-Derived Mesenchymal Stem Cells by T Cell Activation and Inflammation. *Oncol. Rep.* **2013**, *30*, 2211−2219.

(75) Senf, S. M.; Howard, T. M.; Ahn, B.; Ferreira, L. F.; Judge, A. R. Loss of the Inducible Hsp70 Delays the Inflammatory Response to Skeletal Muscle Injury and Severely Impairs Muscle Regeneration. *PLoS One* **2013**, *8*, e62687.

(76) Porter, A. E.; Botelho, C. M.; Lopes, M. A.; Santos, J. D.; Best, S. M.; Bonfield, W. Ultrastructural Comparison of Dissolution and Apatite Precipitation on Hydroxyapatite and Silicon-Substituted Hydroxyapatite in vitro and in vivo. *J. Biomed. Mater. Res., Part A* **2004**, *69*, 670−679.

(77) Li, Y.; Li, Q.; Zhu, S.; Luo, E.; Li, J.; Feng, G.; Liao, Y.; Hu, J. The Effect of Strontium-Substituted Hydroxyapatite Coating on Implant Fixation in Ovariectomized Rats. *Biomaterials* **2010**, *31*, 9006−9014.

(78) Lee, J.; Sayed, N.; Hunter, A.; Au, K. F.; Wong, W. H.; Mocarski, E. S.; Pera, R. R.; Yakubov, E.; Cooke, J. P. Activation of Innate Immunity is Required for Efficient Nuclear Reprogramming. *Cell* **2012**, *151*, 547−588.

(79) Thomas, M. V.; Puleo, D. A. Infection, inflammation, and bone regeneration: a paradoxical relationship. *J. Dent. Res.* **2011**, *90*, 1052−61.

(80) Dalby, M. J.; Gadegaard, N.; Tare, R.; Andar, A.; Riehle, M. O.; Herzyk, P.; Wilkinson, C. D. W; Oreffo, R. O. C. The Control of Human Mesenchymal Cell Differentiation Using Nanoscale Symmetry and Disorder. *Nat. Mater.* **2007**, *6*, 997−1003.

(81) Poole, K.; Khairy, K.; Friedrichs, J.; Franz, C.; Cisneros, D. A.; Howard, J.; Mueller, D. Molecular-scale Topographic Cues Induce the Orientation and Directional Movement of Fibroblasts on Two-Dimensional Collagen Surfaces. *J. Mol. Biol.* **2005**, *349*, 380−386.

(82) Uskoković, V.; Batarni, S. S.; Schweicher, J.; King, A.; Desai, T. A. Effect of Calcium Phosphate Particle Shape and Size on their Antibacterial and Osteogenic Activity in the Delivery of Antibiotics *in Vitro*. *ACS Appl. Mater. Interfaces* **2013**, *5*, 2422−2431.

(83) Uskoković, V. Nanomaterials and Nanotechnologies: Approaching the Crest of this Big Wave. *Curr. Nanosci.* **2008**, *4*, 119−129.

(84) Uskoković, V. Entering the Era of Nanoscience: Time to Be So Small. *J. Biomed. Nanotechnol.* **2013**, *9*, 1441−1470.

(85) Hobbs, R. G.; Petkov, N.; Holmes, J. D. Semiconductor Nanowire Fabrication by Bottom-Up and Top-Down Paradigms. *Chem. Mater.* **2012**, *24*, 1975−1991.

(86) Barth, J. V.; Costantini, G.; Kern, K. Engineering Atomic and Molecular Nanostructures at Surfaces. *Nature* **2005**, *437*, 671−679.